Electronic Supplementary Information

Experimental Section

Materials: Commercial carbon-supported Pt nanoparticles (JM Pt/C, 20 wt.%) were bought from Johnson Matthey. Perchloric acid ($HClO_4$, 72%), potassium phosphate monobasic (KH_2PO_4, 99.99%), potassium phosphate dibasic (K_2HPO_4, 99.99%) were purchased from Beijing Chemical Corporation. Cerium (IV) sulfate ($Ce(SO_4)_2$, 99.9%), isopropyl alcohol (IPA, 99.5%), selenium (Se, 99.99%) powder were purchased from Aladdin Ltd. Nafion solution (5% w/w) was obtained from Sigma-Aldrich Chemical Reagent Co. Ltd. High purity Ar (99.999%), O_2 (99.999%) and H_2/Ar (5%) gas were purchased from Air Liquide Chengdu Co., Ltd. Ultrapure water (18.25 Ω) used throughout all experiments was purified through a Millipore system. All the chemicals were used as received without further purification.

Prepaprtion of $PtSe_2$/C: In a typical synthesis, 20 mg Pt/C nanoparticles were placed in the downstream of a quartz tube with an alumina boat containing 1 g Se powder in the upstream side. The quartz tube was heated at 400 ℃ with a ramp rate of 5 ℃ min^{-1} and kept at 400 ℃ for 2 h in flowing H_2/Ar (5%) gas to transport the vaporized Se to the Pt nanoparticles. During the heating process, Se powder was vaporized to react with Pt nanoparticles for selenization. Finally, the quartz tube was naturally cooled down to room temperature.

Characterization:

XRD patterns were acquired on a Shimadzu XRD-6100 diffractometer with Cu Kα radiation (40 kV, 30 mA) of wavelength 0.154 nm (Japan). SEM images were collected on a GeminiSEM 300 scanning electron microscope (ZEISS, Germany) at an accelerating voltage of 5 kV. XPS measurements were performed on an ESCALABMK II X-ray photoelectron spectrometer using Mg as the exciting source. Raman spectroscopy measurements were performed on a Renishaw 1000 Raman imaging microscope system with an excitation wavelength of 632.8 nm. TEM and HTEM images were collected on a FEI Tecnai G2 F20 SWIN transmission electron microscope operated at 200 kV. In situ attenuated total reflection infrared spectroscopy

measurements were taken on a BRUKER-EQUINOX-55 IR spectrophotometer, a diamond-like carbon was coated onto a Si wafer (5 × 8 × 1 mm^3) to prepare the internal reflection element (IRE). The absorbance data of spectrophotometer were acquired on SHIMADZU UV-1800 UV-Vis spectrophotometer. In situ ATR-FTIR measurements were taken on a BRUKER-EQUINOX-55 IR spectrophotometer, a diamond-like carbon was coated onto a Si wafer (5 × 8 × 1mm^3) to prepare the internal reflection element (IRE). The coated IRE was ultrasonicated for 2 min with 30% concentrated H_2SO_4 followed by rinsing with DI water before experiments. A 50 µL of 2mg mL^{-1} catalyst ink (no Nafion binder) was dropcast on the IRE and dried under air at room temperature. A glassy carbon paper was placed on top of the catalyst layer for good electrical contact. Glassy carbon rod connected to the IRE, Pt gauze, and Ag/AgCl in 3M KCl were used as the working electrode, counter electrode, and reference electrode, respectively. An FTIR spectrometer with a mercury cadmium telluride (MCT) detector was used for the in situ ATR-FTIR measurements. 0.1 M PBS solutions were saturated with O_2 for ORR. Gamry Reference 600 potentiostat during recording of the IR spectra.

Electrochemical measurements:

All the electrochemical experiments were performed on an electrochemical workstation (CHI 760E) in a three-electrode system. For the rotating ring-disk electrode (RRDE) measurements, a glassy carbon electrode with a diameter of 5.6 mm, Ag/AgCl and a platinum plate electrode (1 × 1 cm^2) were employed as working electrode, reference electrode, and counter electrode, respectively. The potentials reported in this experiment were converted to reversible hydrogen electrode (RHE) scale via normalization processing with the following equation: E (vs. RHE) = E (vs. Ag/AgCl) + 0.059 × pH + 0.198 V. The RRDE was polished with different particle size of alumina powder (1 µm and 0.05 µm) for 5 min and ultra-sonicated in ultrapure water for 10 s. The ink was prepared by mixing the catalysts in ultrapure water, isopropyl alcohol (v/v = 4/1) to achieve a catalyst concentration of 5 mg mL^{-1} with 20 µL Nafion solution via sonication for 30 min. Working electrode was obtained through spin-coating (400 rpm) 5 µl of the catalytic ink onto the glassy carbon electrode after natural drying. The H_2O_2 production activity was assessed by LSV with a scan rate of 10 mV s^{-1} under a rotation

speed of 1600 rpm in O_2-saturated 0.1 M PBS and 0.1 M $HClO_4$ electrolytes. During the LSV, the Pt ring potential was fixed at 1.2 V vs. RHE. The H_2O_2 selectivity was calculated using the following relation:

$$H_2O_2\ (\%) = 200 \times (I_{ring} / N)/(I_{disk} + I_{ring} / N)$$

where I_{ring} is the ring current, I_{disk} is the disk current and N is the collection efficiency (0.35 after calibration).

The electron transferred number of per oxygen molecule in the ORR can be calculated by the Koutechy-Levich (K-L) equation (1).

$$1/J = 1/J_k + B^{-1}\omega^{-1/2} \qquad (1)$$

Where J_k is the kinetic current density and ω is the rotation rate. The value of B could be calculated from the slope of Levich equation (2) as follows:

$$B = 0.2nF(D_0)^{2/3}\upsilon^{-1/6}C_0 \qquad (2)$$

Where n is the electron transfer number of per oxygen molecule, F is the Faraday constant (F = 96485 C mol^{-1}), C_0 is the bulk concentration of O_2 (1.2×10^{-1} mol cm^3), D_0 is the diffusion coefficient of O_2 (1.67×10^{-5} cm^2 s^{-1}), υ is the kinetic viscosity (0.01 cm^2 s^{-1}), the constant is 0.2 when the rotation speed unit is represented as rpm.[1]

The electrogeneration of H_2O_2: The electro-generation of H_2O_2 was evaluated in a two-compartment cell with nafion membrane as separator. First, the membrane was protonated by in 5 wt % H_2O_2 aqueous solution at 80 °C for 1 h, then washed with ultrapure water until the pH value of the water returned to neutral, followed by boiling with dilute H_2SO_4 (5 wt%) at 80 °C for 1 h. Finally, the membrane was soaked with ultrapure water for 4 h. The electrochemical experiments were carried out with an electrochemical workstation (CHI 760E) using a three-electrode system. Cathode were prepared by depositing $PtSe_2$/C ink on a carbon paper ($PtSe_2$/C-CP, 0.1 mg cm^{-2}).

To quantify the H_2O_2 produced, the samples were collected at certain time and mixed with same volume of $Ce(SO_4)_2$ solution (0.1 mmol L^{-1}). The H_2O_2 yield was measured by using the indicator of $Ce(SO_4)_2$ ($2Ce^{4+} + H_2O_2 \rightarrow 2Ce^{3+} + 2\ H^+ + O_2$). The generated complex compound solution was detected with UV-vis spectrophotometer. A typical concentration-absorbance curve was calibrated by linear fitting the absorbance values at wavelength length of 320 nm for various known concentration of

0.02, 0.04, 0.06, 0.08, 0.1 mmol L^{-1} of Ce^{4+}. The fitting curve (y = 5.025x – 0031, R^2 = 0.99997) shows good linear relation of absorbance value with H_2O_2 concentration. The yield of H_2O_2 was finally determined based on the reduced Ce^{4+} concentration. The Faradic efficiency (FE) for H_2O_2 generation in H-cell was calculated as follows:

$$FE\% = \frac{\text{mole of generation } H_2O_2 \times 2 \times 96485}{\text{total consumed charge (C)}}$$

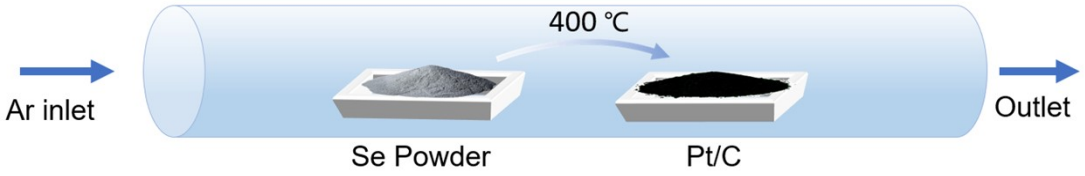

Fig. S1. Schematic of the experimental setup for the selenziation of Pt/C to $PtSe_2$/C.

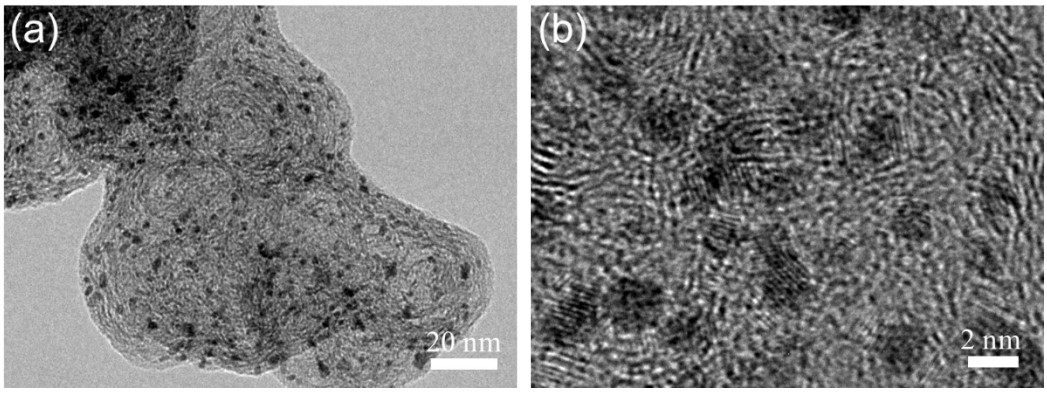

Fig. S2. (a) TEM and (b) high resolution TEM images of commercial Pt/C.

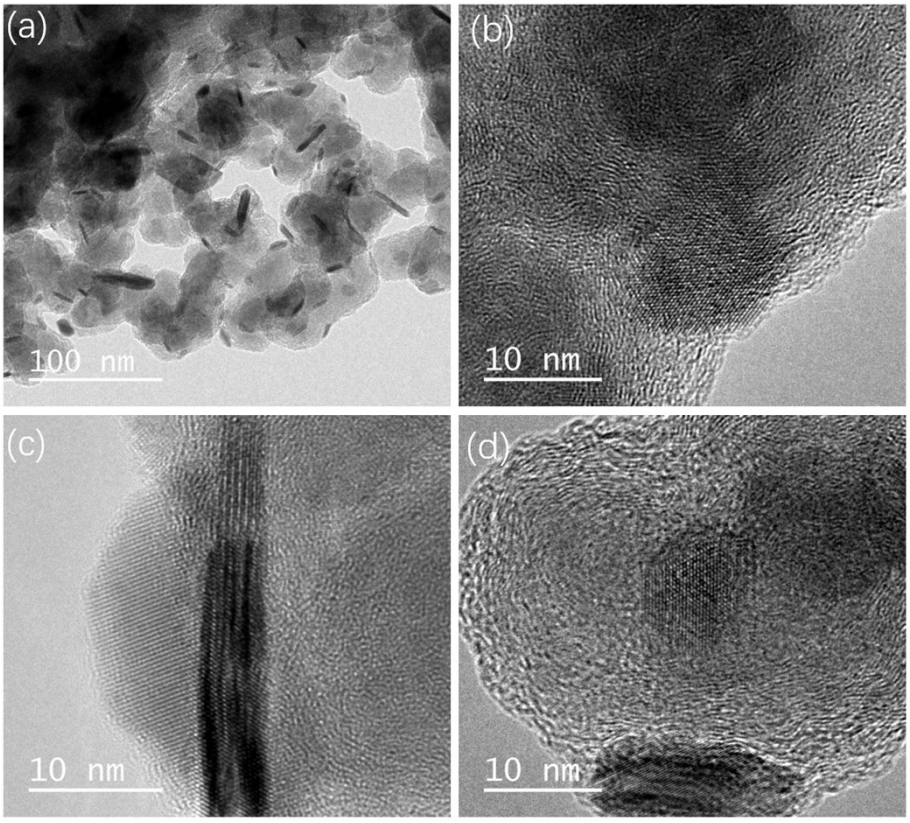

Fig. S3. (a) TEM and (b-d) high resolution TEM images of $PtSe_2$/C.

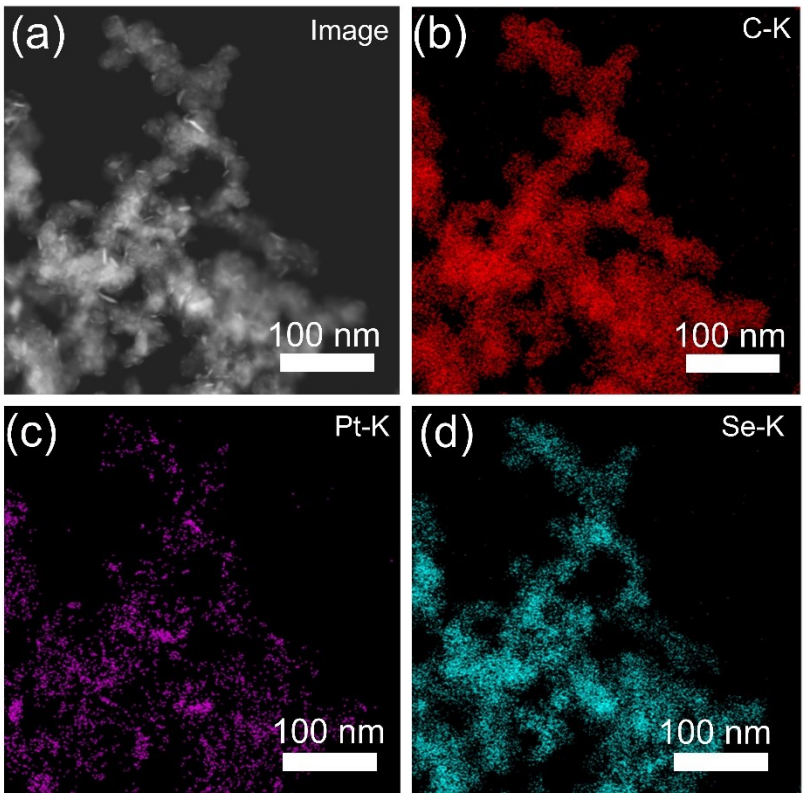

Fig. S4. STEM image (a) and the corresponding EDX elemental mapping images of (b) C, (c) Pt and (d) Se.

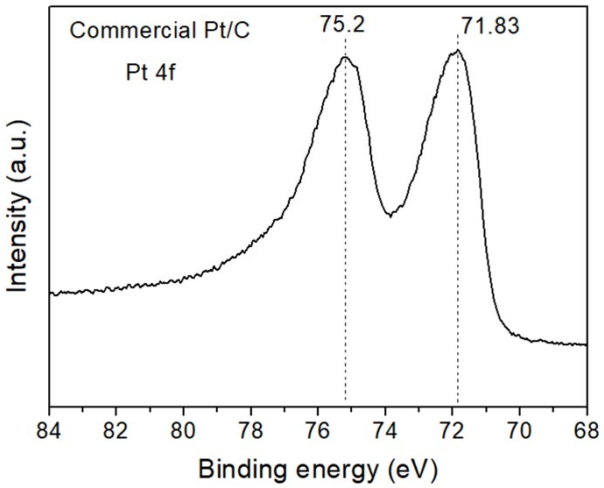

Fig. S5. XPS spectra of commercial Pt/C in the Pt 4f region.

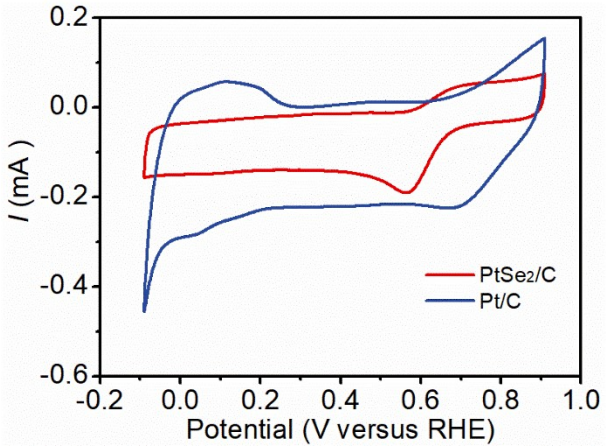

Fig. S6. CV curves of Pt/C and $PtSe_2$/C in O_2-saturated 0.1 M PBS.

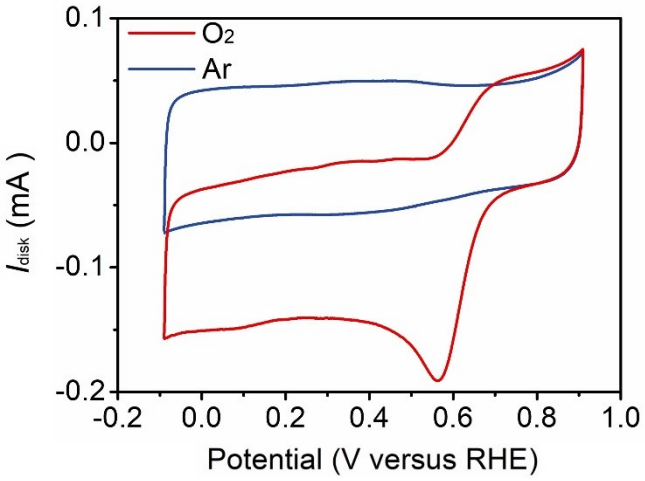

Fig. S7. CV curves of $PtSe_2$/C in Ar and O_2-saturated 0.1 M PBS.

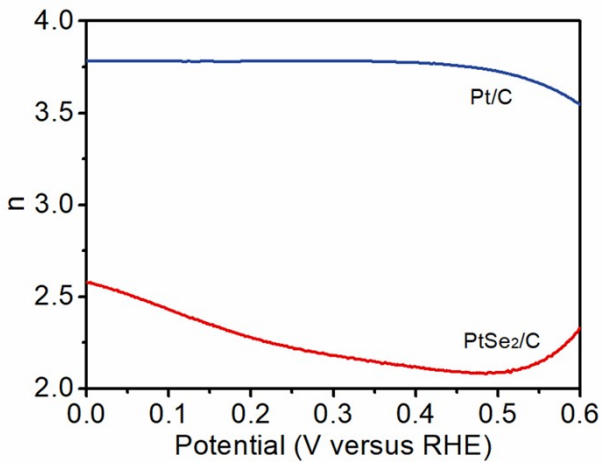

Fig. S8. Calculated electron transfer numbers of Pt/C and $PtSe_2$/C in 0.1 M PBS electrolyte.

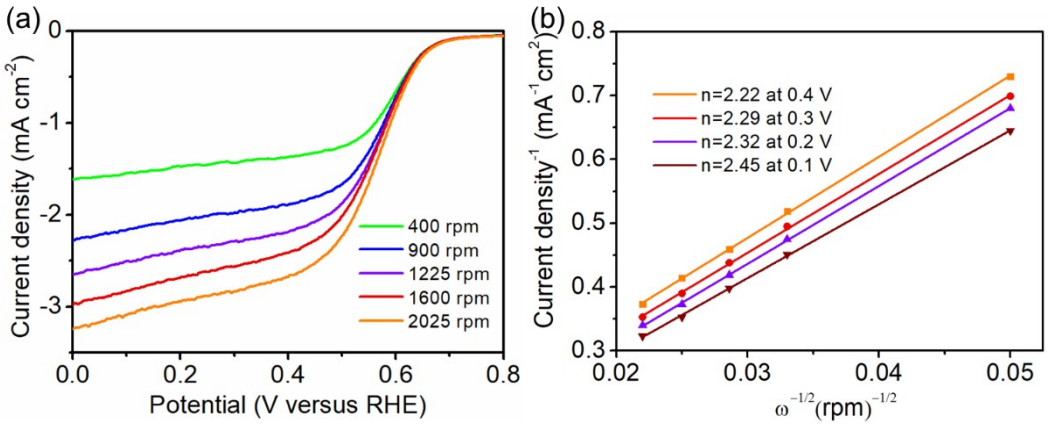

Fig. S9. (a) LSV curves of $PtSe_2$/C at different rotation rates and (b) corresponding Koutecky-Levich plots.

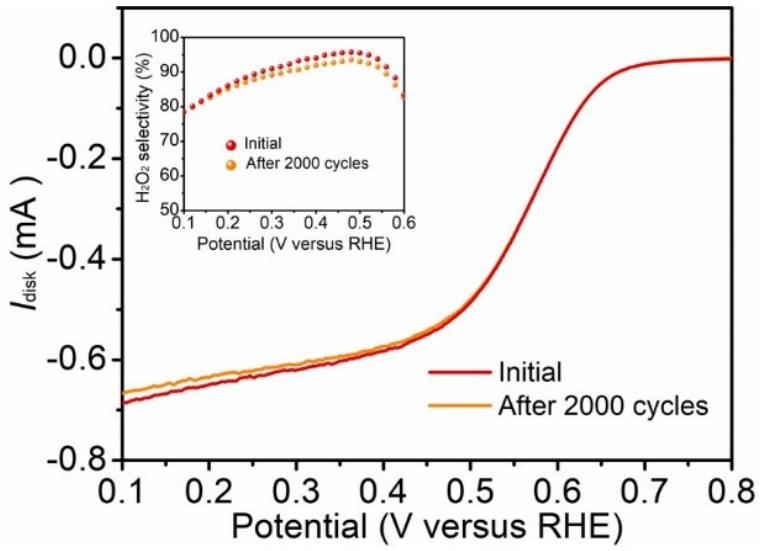

Fig. S10. Stability measurements of $PtSe_2$/C in PBS, the inset represents the selectivity of $PtSe_2$ before and after 2000 CV cycles.

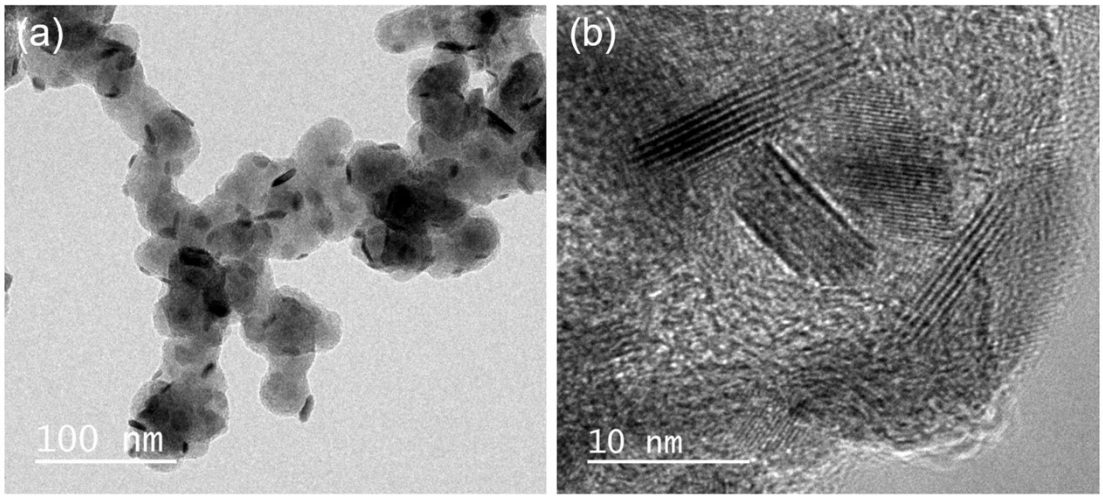

Fig. S11. (a) TEM and (b) high resolution TEM images of $PtSe_2$/C after 2000 cycles.

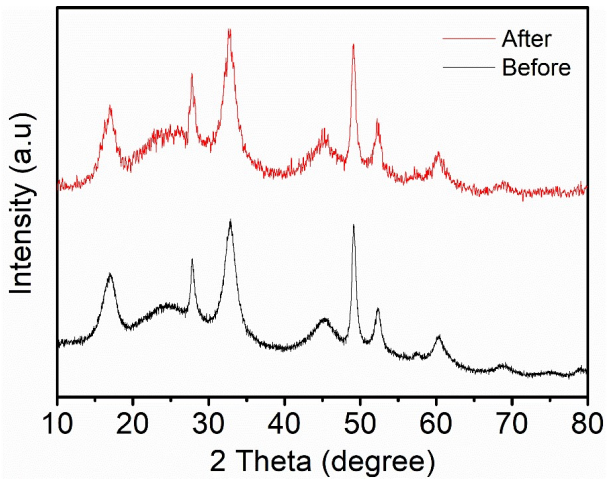

Fig. S12. XRD pattern of $PtSe_2$/C before and after 2000 cycles.

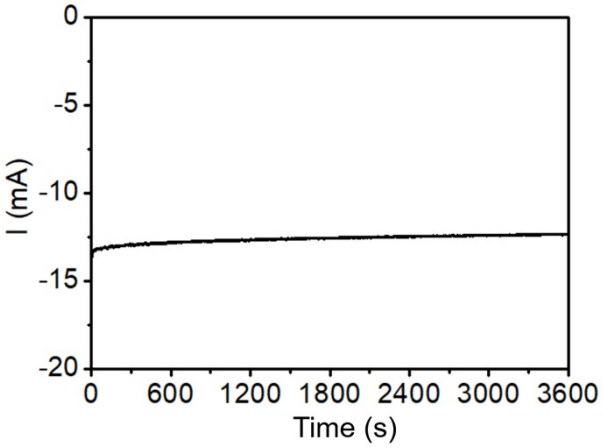

Fig. S13. Time-dependent current curve of $PtSe_2$/C in O_2-saturated 0.1 M PBS at 0.3 V.

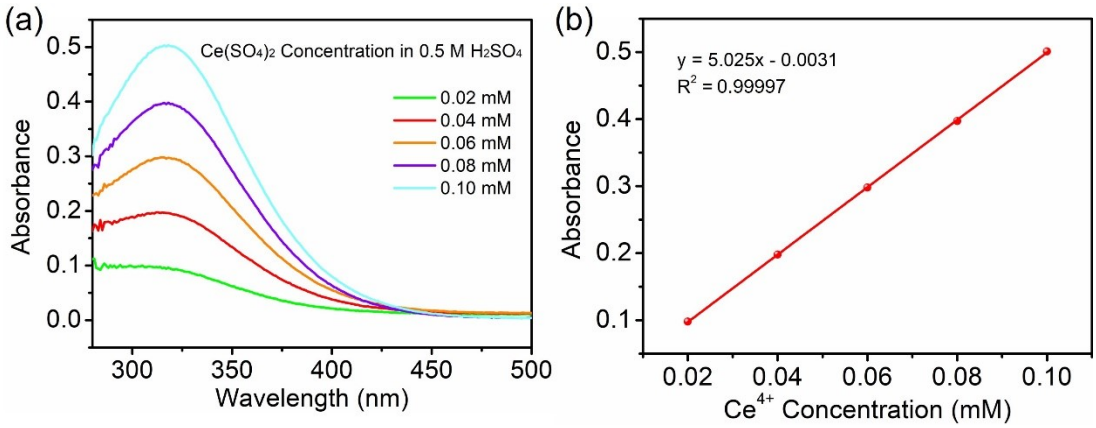

Fig. S14. (a) UV-Vis spectra of Ce^{4+} solution with various concentrations. (b) corresponding standard curve.

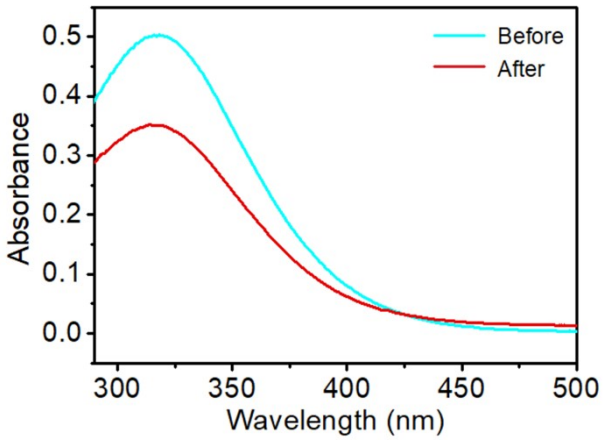

Fig. S15. UV-Vis spectra of the ceric sulfate indicator before and after stained with electrolytes.

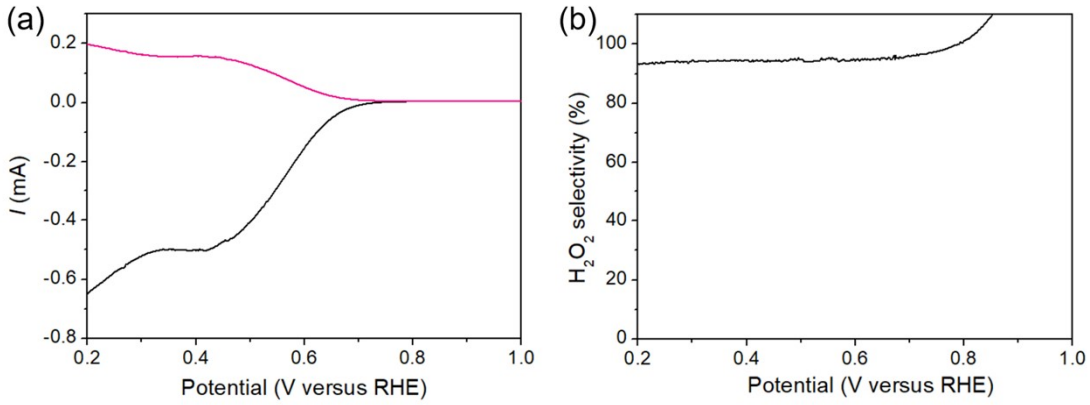

Fig. S16. (a) Polarization curves of $PtSe_2$/C and Pt/C at 1600 rpm in O_2-saturated 0.1 M KOH and (b) corresponding H_2O_2 selectivity.

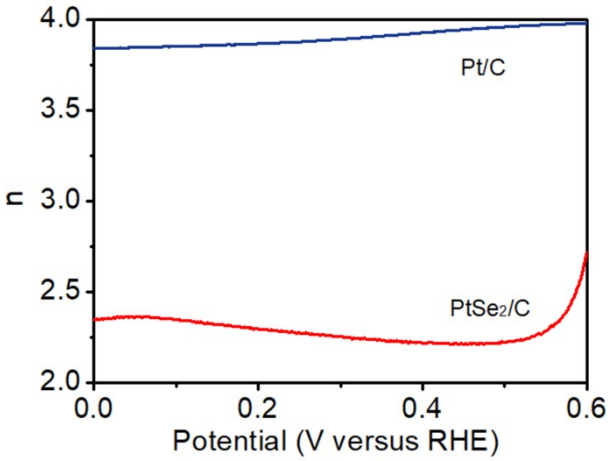

Fig. S17. Calculated electron transfer numbers of Pt/C and $PtSe_2$/C in 0.1 M $HClO_4$ electrolyte.

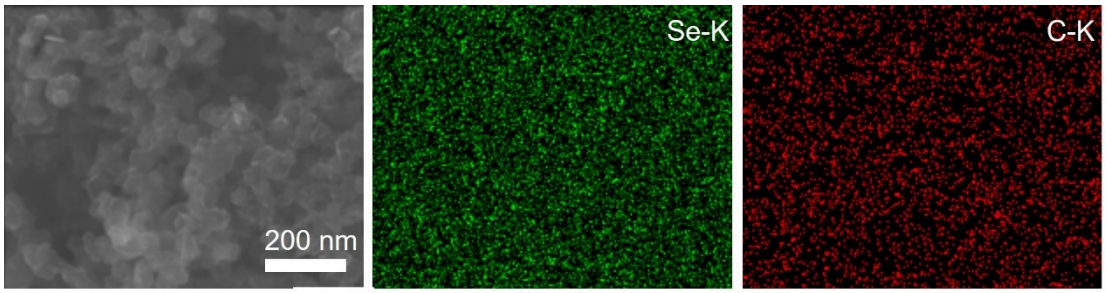

Fig. S18. The EDX elemental mapping images of Se/C.

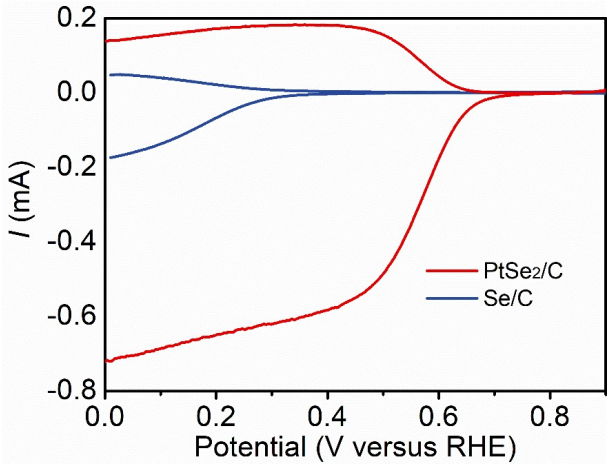

Fig. S19. LSV curves of $PtSe_2$/C and Se/C in O_2-saturated 0.1 M PBS.

Table S1. Comparison of the catalytic performance of $PtSe_2$/C with reported $2e^-$ ORR catalysts.

Electrocatalyst	Electrolyte	Selectivity [%]	Over potential V vs. RHE	Reference
$PtSe_2$/C	0.1 M PBS	94.1	0	This work
	0.1 M $HClO_4$	85.1	0.1	
Au-Pd/C	0.1 M $HClO_4$	93	0.35	2
Pt-Hg/C	0.1 M $HClO_4$	91	0.1	3
Pt1/TiN	0.1 M $HClO_4$	60	0.2	4
Fe-C-O	0.1 M PBS	80	0.2	5
Co1-NG(O)	0.1 M PBS	50	0	6
	0.1 M $HClO_4$	55	0	
VC	0.1 M H_2SO_4	75	0.4	7
Co-NC	0.1 M $HClO_4$	93	0	8
Pt/HSC	0.1 M $HClO_4$	94	0.1	9
Pt/TiC	0.1 M $HClO_4$	68	0.25	10
C(Pt)/C	1 M $HClO_4$	41	0.1	11
Au/C	0.1 M $HClO_4$	80	/	12
$MoTe_2$/Graphene	0.5 M H_2SO_4	90	0.14	13
monodisperse colloidal PtP_2 NCs	0.1 M $HClO_4$	90	0.05	14
Pd_4Se	0.1 M KCl	89.7	0	15

1. C Song, J Zhang. Springer, London, 2008: 89-134. C. Song and J. Zhang, in PEM Fuel Cell Electrocatalysts and Catalysts Layers: Fundamentals and Applications, ed. J. Zhang, Springer, 2008, vol. XXII.
2. J. S. Jirkovský, I. Panas, E. Ahlberg, M. Halasa, S. Romani and D. J. Schiffrin, *J. Am. Chem. Soc.*, 2011, **133**, 19432–19441.
3. S. Siahrostami, A. Verdaguer-Casadevall, M. Karamad, D. Deiana, P. Malacrida, B. Wickman, M. Escudero-Escribano, E. A. Paoli, R. Frydendal, T. W. Hansen, I. Chorkendorff, I. E. L. Stephens and J. Rossmeisl, *Nat. Mater.*, 2013, **12**, 1137–1143.
4. S. Yang, J. Kim, Y. J. Tak, A. Soon and H. Lee, *Angew. Chem. Int. Ed.*, 2016, **55**, 2058–2062.
5. K. Jiang, S. Back, A. J. Akey, C. Xia, Y. Hu, W. Liang, D. Schaak, E. Stavitski, J. K. Nørskov, S. Siahrostami and H. Wang, *Nat. Commun.*, 2019, **10**, 3397.
6. E. Jung, H. Shin, B. H. Lee, V. Efremov, S. Lee, H. S. Lee, J. Kim, W. Hooch Antink, S. Park, K. S. Lee, S. P. Cho, J. S. Yoo, Y. E. Sung and T. Hyeon, *Nat. Mater.*, 2020, **19**, 436–442.
7. A. Wang, A. Bonakdarpour, D. P. Wilkinson and E. Gyenge, *Electrochim. Acta*, 2012, **66**, 222–229.
8. J. Gao, H. bin Yang, X. Huang, S. F. Hung, W. Cai, C. Jia, S. Miao, H. M. Chen, X. Yang, Y. Huang, T. Zhang and B. Liu, *Chem*, 2020, **6**, 658–674.
9. C. H. Choi, M. Kim, H. C. Kwon, S. J. Cho, S. Yun, H. T. Kim, K. J. Mayrhofer, H. Kim and M. Choi, *Nat. Commun*., 2016, **7**, 10922.
10. S. Yang, Y. J. Tak, J. Kim, A. Soon and H. Lee, *ACS Catal*., 2017, 7, 1301–1307.
11. C. H. Choi, H. C. Kwon, S. Yook, H. Shin, H. Kim, M. Choi, *J. Phys. Chem. C*, 2014, **118**, 30063–30070.
12. J. S. Jirkovsky, M. Halasa, D. J. Schiffrin, *Phys. Chem. Chem. Phys.*, 2010, **12**, 8042–8052.
13. X. Zhao, Y. Wang, Y. Da, X. Wang, T. Wang, M. Xu, X. He, W. Zhou, Y. Li, J. N. Coleman, Y. Li, *Natl. Sci. Rev.*, 2020, **7**, 1360–1366.
14. H. Li, P. Wen, D. S. Itanze, Z. D. Hood, S. Adhikari, C. Lu, X. Ma, C. Dun, L.

Jiang, D. L. Carroll, Y. Qiu, S. M. Geyer, *Nat. Commun*., 2020, **11**, 3928.

15. C. Yang, S. Bai, Z. Yu, Y. Feng, B. Huang, Q. Lu, T. Wu, M. Sun, T. Zhu, C. Cheng, L. Zhang, Q. Shao, X. Huang, *Nano Energy*, 2021, **89**, 106480.